ЖЭТФ, 2002, том 122, вып. 4 (10), стр. 723–737

AMPLIFICATION OF SHORT LASER PULSES BY RAMAN BACKSCATTERING IN CAPILLARY PLASMAS

I. Y. Dodin**, G. M. Fraiman

Institute of Applied Physics, Russian Academy of Sciences
603950, Nizhnii Novgorod, Russia

V. M. Malkin, N. J. Fisch

Princeton Plasma Physics Laboratory, Princeton, NJ 08543, USA

Submitted 1 April 2002

Short laser pulses can be significantly amplified in the process of Raman backscattering in plasma inside an oversized dielectric capillary. A dielectric capillary allows obtaining high intensities of the output radiation by sustaining efficient amplification on large distances compared to the diffraction length. The efficiency of the interaction between the pump wave and the amplified pulse is shown to be not critically sensitive to the transverse structure of the wave fields. For a quasi-single-mode initial seed pulse and a low pump intensity, the amplified pulse tends to preserve its transverse structure due to nonlinear competition of the capillary eigenmodes. At a high power of the pump wave, multi-mode amplification always takes place but the growth of the front peak of the pulse still follows the one-dimensional model. The Raman-backscattering instability of the pump wave resulting in the noise amplification can be suppressed in detuned interaction by chirping the pump wave or arranging an inhomogeneous plasma density profile along the trace of amplification. The efficiency of the desired pulse amplification does not significantly depend on detuning in the case of a smooth detuning profile. Density inhomogeneities are shown to exert less influence on the amplification within a capillary than in the one-dimensional problem. Parameters of a future experiment on the Raman amplification of a short laser pulse inside a capillary are proposed.

PACS: 52.35.Mw, 52.38.Bv

1. INTRODUCTION

Laser intensities inside conventional amplifiers are limited to gigawatts (GW=10^9 W) per cm^2, above which a nonlinear modification of the material refraction index causes unacceptable distortions of the laser pulses [1]. The chirp pulse amplification technique allows increasing the output intensities by means of the longitudinal compression of laser pulses after their amplification [2]. The compression is usually performed by means of metallic diffraction gratings, which can survive intensities not larger than tens of TW/cm^2 (TW=10^{12} W) [1]. One of the most promising ways for further increasing the output intensities consists in using the advantages of plasma technology [3]. Replacing all the major elements of the amplification–compression scheme by one element containing fully ionized plasma capable of acting as the stretcher, the nonlinear amplification medium, and the compressor simultaneously, is cheaper and more adequate compared to the extensive development of traditional solid-state devices.

Currently, significant attention is attracted to the problem of generating ultraintense laser pulses in plasmas by means of the Raman backscattering process [3]. In this process, the seed pulse amplification follows the resonant excitation of a plasma wave provided by the beating of the seed pulse and the counter-propagating pump wave. The pump wave energy is primarily in compression of the latter. By means of the resonant mechanism discussed in this paper, the amplified pulse duration can be decreased to the period of Langmuir oscillations. In what follows, we term such pulses as short, which corresponds to a femtosecond laser pulse duration for realistic experimental conditions. (As shown in Ref. [4], amplification of even shorter pulses

*E-mail: idodin@pppl.gov

is possible via Compton backscattering, which remains out of the scope of our study, although represents a process complementary to the Raman interaction of laser waves.)

Compared to its solid-state analogues or plasma amplifiers utilizing the interaction of co-propagating pulses, the scheme allows faster amplification, higher maximum output wave intensities, higher thresholds for developing plasma instabilities, and better limits for the nonlinear pulse compression. Because of a relative simplicity of the experimental implementation, the Raman-backscattering pulse amplification in plasmas can successfully compete with more complicated techniques of generating femtosecond laser pulses [2].

Conventionally, the problem of short laser pulse amplification in the Raman backscattering process in plasmas is considered in the framework of a one-dimensional ($1D$) problem, and the transverse structure of the pulse is neglected [1, 3, 5]. But the transverse effects can become important in the experimental implementation of the amplification scheme and further practical applications. The study of the transverse effects was recently started for the pulse interaction in vacuum [6], where the amplification efficiency is significantly limited by the transverse diffraction of the amplified pulse. An efficient interaction in a boundless medium is only possible on distances small compared to the diffraction (Rayleigh) length $z_R \sim kR^2$, where $k = 2\pi/\lambda$ is a characteristic wavenumber of the seed pulse and R is its characteristic transverse scale. After the amplified pulse passes the distance $z \gg z_R$, diffraction increases the transverse scale of the pulse, and therefore, lowers its intensity, which results in a decrease of the interaction efficiency.

In order to maintain high interaction efficiency at large spatial scales compared to z_R, additional laser pulse focusing must be applied. Because of the high intensities of the amplified radiation, conventional dielectric lenses cannot adequately focuse the amplified pulse. The problems of the refraction index distortion or even the dielectric medium breakdown, which might occur, can be eliminated using the channelling properties of a dielectric capillary that plays the role of an optical waveguide for both the pump wave and the amplified pulse. (A similar technique is often used in other Raman media for pulse amplification with significantly lower wave intensities [7, 8].) In oversized ($R \gg \lambda$) dielectric capillaries, the field amplitude decreases to the edges of the transverse waveguide cross-section and almost equals zero on the inner wall of the tube [9]. Therefore, it is possible to have a field amplitude higher than critical (with respect to the breakdown of the dielectric material of the waveguide walls) in the center of the capillary without damaging its walls. These and other properties of channelling laser pulses in the process of the Raman backscattering amplification within a dielectric capillary are the main subject of this paper.

The paper is organized as follows. In Sec. 2, we give the basic equations describing Raman backscattering in plasmas. In Sec. 3, we revise some aspects of the $1D$ Raman amplification problem. We consider the capillary problem in Sec. 4, where we develop a mode approach allowing quantitative and simple qualitative understanding of some phenomena occuring during the laser pulse interaction inside a capillary. We also generalize the conventional $1D$ linear theory of pulse amplification by considering the interaction between the capillary modes of the amplified pulse and discuss some aspects of selective mode discrimination in capillaries. Single- and multi-mode amplification regimes are discussed in Sec. 5 in detail. In Sec. 6, we discuss the problem of detuned amplification. Some numerical estimates and the summary of the main ideas are given in Sec. 7. Specific features of the cylindric dielectric capillary are discussed in the Appendix.

2. BASIC EQUATIONS

Equations for vector electric fields describing paraxial propagation of laser pulses along the z axis can be written as (see, e.g., Refs. [10, 11])

$$\partial_t \mathbf{a} + c\partial_z \mathbf{a} - \frac{ic^2}{2\omega_a}\nabla_\perp^2 \mathbf{a} = \omega_p \mathbf{b} f, \tag{1}$$

$$\partial_t \mathbf{b} - c\partial_z \mathbf{b} - \frac{ic^2}{2\omega_b}\nabla_\perp^2 \mathbf{b} = -\omega_p \mathbf{a} f^*, \tag{2}$$

$$\partial_t f + i\delta\omega f = -\frac{\omega}{2}\mathbf{b}^\dagger \cdot \mathbf{a}, \tag{3}$$

where the vectors $\mathbf{a}$ and $\mathbf{b}$ represent the slowly changing amplitudes of the respective electric fields

$$\begin{aligned} \mathbf{E}_a &= \frac{m_e c\omega_a}{e}\{i\mathbf{a}\exp(ik_a z - i\omega_a t) + \text{c.c.}\}, \\ \mathbf{E}_b &= \frac{m_e c\omega_b}{e}\{i\mathbf{b}\exp(ik_b z - i\omega_b t) + \text{c.c.}\} \end{aligned} \tag{4}$$

of the pump and the seed pulse, and f is the normalized potential of the plasma wave electric field

$$\mathbf{E}_f = \mathbf{k}_f^{(0)}\frac{m_e c\omega_p}{e}\{f\exp(ik_f z - i\omega_f t) + \text{c.c.}\}, \tag{5}$$

where

$$\mathbf{k}_f^{(0)} = \mathbf{k}_f/k_f, \quad \mathbf{k}_f = \mathbf{z}^{(0)}(k_a - k_b),$$

$$\omega_f = \omega_a - \omega_b = \omega_p - \delta\omega.$$

Here,

$$\omega_p = \sqrt{\frac{4\pi n_e e^2}{m_e}}$$

is the plasma frequency, n_e is the electron density, and e and m_e are the electron charge and mass respectively. We assume the rare plasma conditions ($\omega_p \ll \omega_a \approx \omega_b \equiv \omega$) and $k_f \lambda_D \ll 1$, and therefore, $k_{a,b} \approx \omega_{a,b}/c$ and the dispersion of plasma waves can be neglected ($\partial_k \omega_f \approx 0$). In terms of the dimensionless amplitude a, the pump intensity is

$$I_a = \pi c (m_e c^2/e)^2 |a|^2/\lambda^2 = \\ = 2.736 \cdot 10^{18} |a|^2/\lambda^2 \ [\mu\text{m}] \ \text{W/cm}^2,$$

see Ref. [6].

It is useful to introduce the dimensionless equations

$$\partial_\tau \mathbf{a} + \partial_z \mathbf{a} - i(1+\sigma)\nabla_\perp^2 \mathbf{a} = \mathbf{b} f, \tag{6}$$

$$\partial_\tau \mathbf{b} - \partial_z \mathbf{b} - i\nabla_\perp^2 \mathbf{b} = -\mathbf{a} f^*, \tag{7}$$

$$\partial_\tau f + i\delta\omega f = -\mathbf{b}^\dagger \cdot \mathbf{a}, \tag{8}$$

where

$$\sigma = \frac{\omega_a - \omega_b}{\omega_b} \sim \frac{\omega_p}{\omega} \ll 1,$$

the time τ is measured in the units $t_0 = \sqrt{2/\omega\omega_p}$, the longitudinal coordinate z is measured in the units ct_0, f is measured in $\sqrt{\omega/2\omega_p}$, the transverse coordinate ρ is measured in the units $c(2\omega_p\omega^3)^{-1/4}$, and the detuning $\delta\omega$ is measured in the units t_0^{-1}.

For further analysis, it is convenient to introduce the coordinate $\zeta = \tau + z$ (in what follows, this change of variables is called the shift to the reference frame moving together with the amplified pulse at the speed of light). To describe the strongly nonlinear regime of the amplification of a compressed pulse, it suffices to keep only the ζ-derivatives of $\mathbf{a}$ and f (the so-called quasistatic approximation [1, 3]); the basic equations then become

$$2\partial_\zeta \mathbf{a} - i(1+\sigma)\nabla_\perp^2 \mathbf{a} = \mathbf{b} f, \tag{9}$$

$$\partial_\tau \mathbf{b} - i\nabla_\perp^2 \mathbf{b} = -\mathbf{a} f^*, \tag{10}$$

$$\partial_\zeta f + i\delta\omega f = -\mathbf{b}^\dagger \cdot \mathbf{a}. \tag{11}$$

In the case of zero detuning, the basic equations are invariant under the transformation

$$\mathbf{a} \to C\mathbf{a}, \quad \mathbf{b} \to C\mathbf{b},$$

$$f \to Cf, \quad \tau \to \tau/C, \quad \zeta \to \zeta/C, \quad \rho \to \rho/\sqrt{C}.$$

Therefore, the specific value of the pump amplitude $a_0 = a(z \to -\infty)$ is in fact not important in the sense that the field dynamics for another value of a_0 can be obtained by a simple rescaling.

3. THE ONE-DIMENSIONAL PROBLEM

For better understanding of the qualitative phenomena to be discussed in relation to the Raman backscattering inside a capillary, it is useful to revise the basic aspects of the conventional $1D$ problem first (see Refs. [1, 3] for a detailed discussion). During the linear stage of amplification, when the pump depletion is negligible, $a \approx a_0 = \text{const}$, the solution of Eqs. (6)–(8) can be obtained by the Laplace transformation and is given by [1]

$$\begin{aligned} b(\zeta, z) &= \frac{\partial}{\partial\zeta} \int G(\zeta - \zeta', z) b(\zeta', 0) d\zeta', \\ G(\zeta, z) &= I_0(2\sqrt{\eta}), \\ \eta &= -a_0^2 \zeta z, \end{aligned} \tag{12}$$

where we assume zero detuning (a constant detuning can be removed from the evolution equations; the case of the linear detuning $\partial_z \delta\omega = \text{const}$ is considered in Refs. [1, 5] in detail). We note that the spatial coordinate $-z$ plays the role of time in Eqs. (12) measuring the interval between the initial and the current positions of the amplified pulse propagating along the z axis with a fixed velocity equal to the speed of light.

For $\eta \gg 1$, we have

$$G \approx \exp(2\sqrt{\eta})/2\sqrt{\pi\sqrt{\eta}}.$$

In the original variables,

$$\eta = a_0^2 \omega\omega_p (t + z/c)(-z)/2c,$$

and the maximum of G is therefore reached at $z = -ct/2$; it increases with the peak growth rate $\gamma = a_0\sqrt{\omega\omega_p/2}$ as $\exp(\gamma t)$.

Linear approximation (12) is valid until

$$\epsilon(\tau) = \int b(z, \tau) dz$$

remains small compared to unity; a nonlinear solution is formed for larger ϵ. Because of the pump depletion, only the front part of the seed pulse is then amplified, which leads to the effective compression of the pulse. Eventually, as the pulse becomes sufficiently short, the quasistatic approximation (Eqs. (9)–(11))

becomes valid, and for the real constant pump, the solution is therefore given by

$$\begin{aligned} a &= a_0 \cos(U/2), \\ f &= -\sqrt{2} a_0 \sin(U/2), \\ b &= \partial_\zeta U/\sqrt{2}, \end{aligned} \tag{13}$$

where U satisfies the sine-Gordon equation

$$\partial^2_{\tau\zeta} U = a_0^2 \sin U. \tag{14}$$

Equation (14) has a family of self-similar solutions (Fig. 1) $U(\tau,\zeta) = U(\eta)$ that satisfy the equations

$$\eta U_{\eta\eta} + U_\eta = \sin U, \tag{15}$$

or

$$U_{\xi\xi} + U_\xi/\xi = \sin U, \quad \xi = 2\sqrt{\eta}, \tag{16}$$

where we equate η with $a_0^2 \tau\zeta$ because of the quasistatic approximation. It is convenient to consider the solution of Eq. (16) in the plane (U, U_ξ), which can approximately be treated as the phase plane of a nonlinear oscillator with the effective dissipation determined by the term U_ξ/ξ (Fig. 1). The absolute maximum of the self-similar solution grows in time as

$$b_{max} \approx a_0^2 \tau (1 + \ln(4\sqrt{2\pi}/\epsilon_0))^{-1}, \quad \epsilon_0 \equiv \epsilon(0) \ll 1,$$

and the locations of the pulse maxima change as

$$\zeta_{max} \sim 1/b_{max}.$$

The self-similar solution $U(\eta)$ in Eqs. (15), (16) corresponds to the initial conditions

$$b(z, \tau = 0) \equiv b_0(z) = \epsilon_0 \delta(z), \tag{17}$$

which imply that

$$U(\xi = 0+) = \epsilon_0, \quad U'(\xi = 0+) = 0,$$

and which are therefore applicable for all ζ to the left of the initial location of the seed pulse in the frame moving together with the amplified pulse. We now consider what happens when the spatial scale of the amplified pulse $\Delta(\tau)$ becomes comparable to its initial spatial scale $\Delta_0 \equiv \Delta(0)$ and the delta-approximation for initial conditions (17) therefore becomes invalid. In this case,

$$\epsilon_0 = \int_{-\infty}^{+\infty} b_0(z')\, dz'$$

does not determine the solution, and new initial conditions for a self-similar profile must then be applied. The front pulse faces the unperturbed profile of the pump wave. Qualitatively, pump depletion becomes significant ($\delta a/a_0 \sim 1$) starting only with $\zeta = \zeta_*$, where ζ_* is determined by the condition $\epsilon(\zeta_*(\tau)) \sim 1$, with

$$\epsilon(\zeta) = \int_{-\infty}^{\zeta} b(\zeta', \tau) d\zeta'. \tag{18}$$

(To make a rough estimate, we can equate ζ_* to the location of the first maximum of $b(\zeta, \tau)$ at a current instant τ.) Therefore, linear solution (12) remains valid for $\zeta < \zeta_*$. In the case where the spatial scale of the Green's function G is large compared to the spatial scale of the initial pulse, Eq. (12) can be written as

$$U = \epsilon(\zeta) G(\eta). \tag{19}$$

On the other hand, because the self-similar solution represents an attractor, its formation still occurs starting from the end of the linear stage, where its profile can be obtained from linearized Eq. (15) and is given by

$$U = \epsilon_{eff} G(\eta), \tag{20}$$

where ϵ_{eff} is some constant. At the location where the linear stage ends and the self-similar solution starts, i.e., at $\zeta = \zeta_*(\tau)$, the two solutions in Eqs. (19) and (20) must match, which defines $\epsilon_{eff}(\tau)$,

$$\epsilon_{eff}(\tau) = \epsilon(\zeta_*(\tau)). \tag{21}$$

As long as $\Delta(\tau) \gg \Delta_0$, we have

$$\epsilon_{eff} \approx \epsilon_0 = \text{const}.$$

But when the nonlinear compression makes $\Delta(\tau)$ comparable to or less than Δ_0, ϵ_{eff} can become significantly smaller than ϵ_0. If $\epsilon_{eff}(\tau)$ is changing sufficiently slowly, such that the self-similar profile has enough time to set up on the entire length of the pulse, the entire solution remains close to the self-similar one with the only change that it is now parameterized by time-dependent quantity (21) (Fig. 2). But if $\epsilon_{eff}(\tau)$ is changing fast, the self-similar solution may not be able to form, and therefore, does not represent an attractor. Stochastic behavior of the amplified pulse structure is observed in this case.

In the approximation of geometric optics, when the pulse propagation is considered at small distances compared to the Rayleigh length $z_R \sim kR^2$, the diffraction-caused distortion of the transverse structure of laser pulses can be neglected. In this case, $1D$ quasi-self-similar solutions are formed on geometric rays constituting the field of the amplified pulse. The spatial profiles of the amplified pulse that are then formed have a

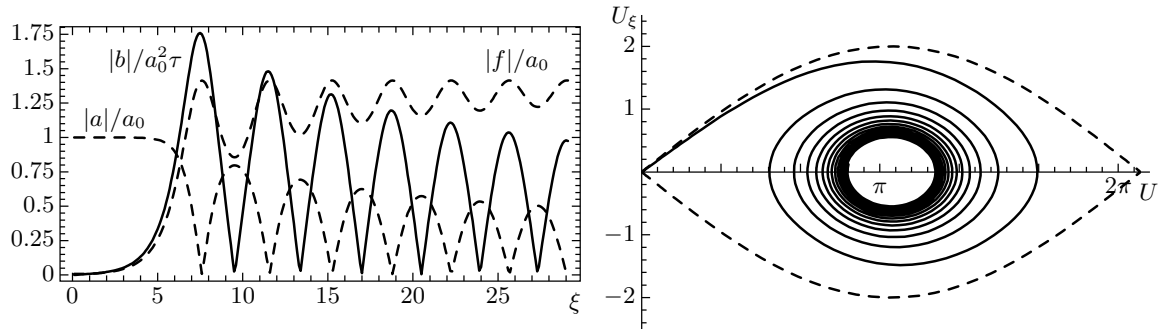

Fig. 1. Self-similar profiles of $|a(\xi)|/a_0$ (dotted decay), $|f(\xi)|/a_0$ (dotted growth), $|b(\xi)|/\tau a_0^2$ (solid line) for $\epsilon_0 = 0.01$ and the behavior of the self-similar solution on the (U,U_ξ) plane (dashed line represents the solution without the «friction» term U_ξ/ξ); $\xi = 2(a_0^2\omega\omega_p(t+z/c)(-z)/2c)^{1/2}$

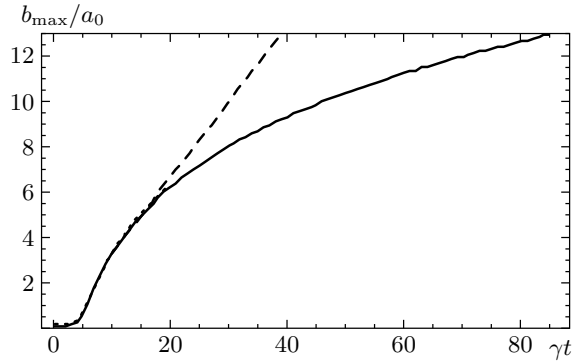

Fig. 2. The amplitude of the amplified $1D$ pulse maximum normalized to the amplitude of the pump wave ($b_{max}/|a_0|$) as a function of $\gamma t \equiv |a_0|\tau$ for $b_0(z) = \epsilon_0 \exp(-z^2/z_0^2)/\sqrt{\pi}z_0$: a delta-shaped initial pulse ($z_0 \to 0$, self-similar profile with fixed $\epsilon_0 = 1.3 \cdot 10^{-2}$, dashed line) and a finite-width initial pulse ($z_0 = \sqrt{5}$, quasi-self-similar profile with $\epsilon_{eff}(\tau)$, solid line)

shape similar to nested horseshoes. But for pulse traces $z > z_R$, the diffraction terms in Eqs. (6)–(11) become significant and must therefore be taken into account (see Sec. 5).

4. THE MODE APPROACH TO THE NON-ONE-DIMENSIONAL PROBLEM

We consider the pump wave $\mathbf{a}$ and the amplified pulse $\mathbf{b}$ given by a series in the normalized eigenmodes $\boldsymbol{\psi}_s$, $\langle\boldsymbol{\psi}_m|\boldsymbol{\psi}_n\rangle = \delta_{mn}$,

$$\begin{aligned}\mathbf{a} &= R\sum_n a_n(z,\tau)\boldsymbol{\psi}_n(\mathbf{r}_\perp),\\ \mathbf{b} &= R\sum_m b_m(z,\tau)\boldsymbol{\psi}_n(\mathbf{r}_\perp),\end{aligned} \tag{22}$$

where R is the radius of the capillary, which we include as a normalization factor to make the amplitudes a_n and b_m dimensionless (see the Appendix for the explicit form of $\boldsymbol{\psi}_n$ for a dielectric capillary). By definition, the eigenfunctions $\boldsymbol{\psi}_s$ satisfy the equation

$$\nabla_\perp^2\boldsymbol{\psi}_s + \chi_s^2\boldsymbol{\psi}_n = 0, \tag{23}$$

where χ_s is the transverse wavenumber of the s-th eigenmode. From Eqs. (6)–(8), we obtain the equations for the amplitudes a_n and b_m,

$$(\partial_\tau + \partial_z + i\delta\Omega_n^{(a)})a_n = \sum_m f_{nm}b_m, \tag{24}$$

$$(\partial_\tau - \partial_z + i\delta\Omega_n^{(b)})b_m = -\sum_n a_n f_{nm}^*, \tag{25}$$

where

$$\delta\Omega_n^{(a)} = \chi_n^2(1+\sigma), \quad \delta\Omega_m^{(b)} = \chi_m^2$$

(or $\delta\Omega_n^{(a,b)} = (c\chi_n)^2/2\omega_{a,b}$ in dimensional variables) and

$$f_{nm} = \langle\boldsymbol{\psi}_n|f|\boldsymbol{\psi}_m\rangle$$

are dimensionless transverse moments of the plasma wave profile satisfying

$$(\partial_\tau + i\delta\omega)f_{nm} = -\sum_{k,\,l} C_{nklm}a_l b_k^*, \tag{26}$$

with constant dimensionless coefficients given by

$$\begin{aligned}C_{nklm} &= R^2\langle\boldsymbol{\psi}_n|\boldsymbol{\psi}_k^\dagger\cdot\boldsymbol{\psi}_l|\boldsymbol{\psi}_m\rangle =\\ &= R^2\int d^2r_\perp(\boldsymbol{\psi}_n^\dagger\cdot\boldsymbol{\psi}_m)(\boldsymbol{\psi}_k^\dagger\cdot\boldsymbol{\psi}_l).\end{aligned} \tag{27}$$

The eigenmode approach can be useful only in the case where the modes are coupled weakly, which corresponds to the case of a strong waveguide dispersion. Otherwise, the number of modes to be taken

into consideration becomes infinite. If the characteristic trace z_0 of the pulse evolution is large compared to the Rayleigh length z_R, Eq. (26) can be reduced to

$$(\partial_\tau + i\delta\omega)f_{nm} = -\frac{C_{nm}}{1+\delta_{nm}}(a_n b_m^* + a_m b_n^*), \qquad C_{nm} \equiv C_{nmnm} \geq 0, \tag{28}$$

where we assume the eigenfunctions to contain complexity in polarization factors at most, but not in the functional dependence of the transverse coordinates (for simplicity, below we ignore the fact that C_{nm} can be equal to zero for modes of the opposite polarization). Equations (24), (25), and (28) represent a completely defined Lagrangian set of equations that can be used for obtaining the amplitudes of resonantly interacting modes of the three waves $\mathbf{a}$, $\mathbf{b}$, and f in the case of weak coupling (see below).

The important conclusion following from Eqs. (24), (25), and (28) is that for every pair of modes of the pump and the seed, a_n and b_m, the resonant plasma wave harmonic f_{nm} can be generated to provide coupling of the two electromagnetic waves. This is a specific feature of light scattering on a cold plasma wave for which the spatial resonance condition

$$\mathbf{k}_a = \mathbf{k}_b + \mathbf{k}_f$$

is satisfied automatically because the wavevector $\mathbf{k}_f$ remains arbitrary for the given frequency $\omega_f \approx \omega_p$. For the scattering on any other low-frequency wave f for which the wavevector depends on its frequency ω_f, the multiple mode interaction on the quadratic nonlinearity is impossible.

The presence of the $a_m b_n^*$ term in Eq. (28) is responsible for a possible parasitic resonance, which can be explained as follows. We consider the interaction between the n-th mode of the pump a_n and the m-th mode of the seed pulse b_m generating the resonant plasma wave f_{nm} with the longitudinal wavenumber

$$h_{nm} = k_a - k_b - \delta\Omega_n^{(a)} - \delta\Omega_m^{(b)}.$$

For very small $\sigma \sim \omega_p/\omega_b$ (namely, for $\sigma \lesssim z_R/z_0$, where z_0 is the characteristic spatial scale of the pulse evolution), we have $h_{nm} \approx h_{mn}$, where h_{mn} is the wavenumber of the plasma wave f_{mn} resonant to the beating wave of the modes a_m and b_n, which provides an additional coupling of these two pairs of electromagnetic waves. For example, in the case where the pump contains the modes a_1 and a_2 and the seed pulse contains only b_1, the second seed harmonic $b_2 = O(a_2^* a_1 b_1)$ is generated. This effect can already become important at the linear stage of the interaction in a multi-mode pump, because it alters the increments of the linear Raman amplification.

We now use the developed mode approach to consider the linear stage of the pulse amplification inside a capillary in terms of the equation

$$\partial_\tau(\partial_\tau - \partial_z - i\nabla_\perp^2)\mathbf{b} = \mathbf{a}(\mathbf{a}^\dagger \cdot \mathbf{b}) \tag{29}$$

which directly follows from Eqs. (7) and (8) with zero detuning $\delta\omega$ and with a constant pump $\mathbf{a}$. The right-hand side of Eq. (29) can be considered as the result of applying the linear operator $\widehat{\mathbf{A}} = \mathbf{a}\mathbf{a}^\dagger$ to the vector $\mathbf{b}$, and therefore, Eq. (29) can be rewritten as

$$\left[\partial_\tau(\partial_\tau - \partial_z + i\delta\Omega_m^{(b)}) - \gamma_m^2\right] b_m = \sum_{n\neq m} A_{mn} b_n, \qquad A_{mn} = \langle \boldsymbol{\psi}_m | \widehat{\mathbf{A}} | \boldsymbol{\psi}_n \rangle, \tag{30}$$

where $\gamma_m = \sqrt{A_{mm}}$ represents the increment of the linear amplification of the m-th partial waveguide mode. In an arbitrary waveguide, for a single-mode pump, $a_n = \delta_{ns} a$, the matrix elements A_{mn} are of the order of a^2 for $n, m \sim 1$ and $A_{mn} = A(|m-n|)$ for $n, m \gg 1$, where the function $A(k) \sim a^2$ for $k \sim 1$ and decays as its argument grows.

The eigenmodes of the empty waveguide are coupled via the pump inhomogeneity. Only for the uniform pump, the matrix A_{mn} is diagonal and the right-hand side of Eq. (30) is therefore zero. For a nonuniform pump, which is only possible inside a capillary, the effect of mode coupling always occurs. In the case of a weak interaction ($\gamma_m \ll \delta\Omega_m^{(b)}$), the eigenwaves of system (30) are close to its partial waves, and the increments of the eigenwaves are approximately given by γ_m, $m = 1, 2, \ldots \infty$ (here, we neglect the effect of the parasitic resonance discussed above). For the single-mode pump, $a_n = \delta_{ns} a$, all the increments are of the order of a and are independent of m for $m \gg s$. Specifically, for pulse amplification on the lowest mode of the pump in a dielectric capillary, $s = 1$, we have

$$\frac{\gamma_m - \gamma_1}{\gamma_1} < 0.16.$$

Hence, the increments of amplication of all the waveguide modes are close to each other at the linear stage of interaction.

Variations of the pump transverse structure do not change the interaction efficiency significantly. For example, without the possible parasitic resonance taken into account, the amplification increment of the m-th

partial mode (equal to the increment of the m-th eigenmode in the case of weak interaction) is given by

$$\gamma_m = \sqrt{\sum_n C_{nm}|a_n|^2}, \tag{31}$$

which implies that each mode of the pump amplifies each mode of the seed, because $C_{nm} > 0$ for all n and m. The higher modes of the pump amplify the seed with approximately the same efficiency as the lower ones, because

$$C_{nm}/C_{mm} \approx \text{const} \sim 1 \quad \text{for} \quad n \gg m.$$

This effect originates in the fact that the wave interaction inside a capillary is not a three-wave but a multiwave process, where the effective energy exchange between every pair of the pump and the seed modes is possible.

Because the increments of the linear amplification are approximately the same for all waveguide modes, the linear stage of pulse amplification cannot provide significant enhancement of the signal-to-noise ratio. This is true, however, only if the energy losses (which have not been taken into account yet) are negligible at the distance of pulse propagation, which might not be the case in real experiments. In an oversized cylindrical dielectric capillary, the energy losses are mostly radiative and can be incorporated into the model by introducing the spatial decrements of individual modes [9],

$$\alpha_{nm} \sim \left(\frac{\mu_{m,\,n}}{2\pi}\right)^2 \frac{\lambda^2}{R^3} \tag{32}$$

(see the Appendix for the notation). The spatial scale of the exponential decay α_s^{-1} decreases with the mode number s roughly as s^{-2}, and for $\gamma_1 \gtrapprox \alpha_1$, only the lowest mode can be amplified and the amplification of the higher modes is suppressed. This implies that the radiative energy losses essentially result in a selective mode discrimination, which can provide the single-mode operation regime.

Additional mode discrimination can occur in relatively narrow waveguides, where the group velocity substantially differs from mode to mode. After the amplified pulse passes the distance $z \gtrsim L_{pulse}(kR)^2$, where L_{pulse} is the length of the pulse, the wave envelope corresponding to the lowest mode leaves the envelopes of the higher modes behind. The front envelope then has a preferential opportunity of absorbing the energy from the pump wave. Because the pump is significantly depleted by the lowest mode, the higher ones are left with less energy to absorb, which also maintains the single-mode amplification regime.

5. SINGLE- AND MULTI-MODE AMPLIFICATION

The condition of a weak interaction (or the condition of a strong waveguide dispersion)

$$\gamma \ll \delta\Omega^{(b)},$$

$$a \ll a_{crit}, \quad a_{crit} = \sqrt{2/\omega\omega_p}(c\chi)^2/2\omega, \quad \chi = \pi/R,$$

can be treated as follows. The increment of the pulse amplification $\gamma \sim a\sqrt{\omega\omega_p}$ determines the spread of the amplified pulse spectrum $\delta h \sim \gamma/c$. As long as δh remains small compared to the spectral gap between the individual modes,

$$\Delta h \sim \delta\Omega^{(b)}/c \sim 1/kR^2,$$

the waveguide eigenmodes do not overlap, and hence, represent a good basis for developing the mode approach in the linear theory. In this case, the eigenmodes of coupled system (30) remain close to the partial waves of the empty waveguide. This implies that an initially single-mode seed pulse remains single-mode on the entire duration of the linear stage.

The next question is what happens after the linear stage, when nonlinear compression comes into play providing its own spectrum broadening. We consider the single-mode initial conditions for the seed pulse, e.g., $b_m^{(0)} = b_1^{(0)}\delta_{m1}$. Until the end of the linear stage, the higher mode amplitudes remain small compared to b_1. Then, it is the mode b_1 that passes from the linear to the nonlinear regime first, because its amplitude is the largest. (Here, by the nonlinear regime of an individual mode, we mean the ability of this particular mode to deplete the pump, which might have already been distorted by other modes at the moment.) In the laboratory frame, the maximum of the wave envelope moves approximately with the speed of light in the nonlinear regime, but in the linear one, the effective pulse velocity is sufficiently lower. For example, as follows from the linear theory of pulse propagation in a constant pump (Sec. 3), the maximum travels with the speed equal to half the speed of light. The higher mode envelopes (remaining in the linear regime) are therefore left behind the envelope of the first mode. The effective amplitude of the pump $a_{eff} < a_0$ determining the increments of the higher modes is decreased by the first mode. Because the first mode suppresses the growth of the higher modes, the waveguide dispersion effectively results in a nonlinear competition of the modes tending to sustain the single-mode operation. We call this effect the mode elasticity, because the strongest mode

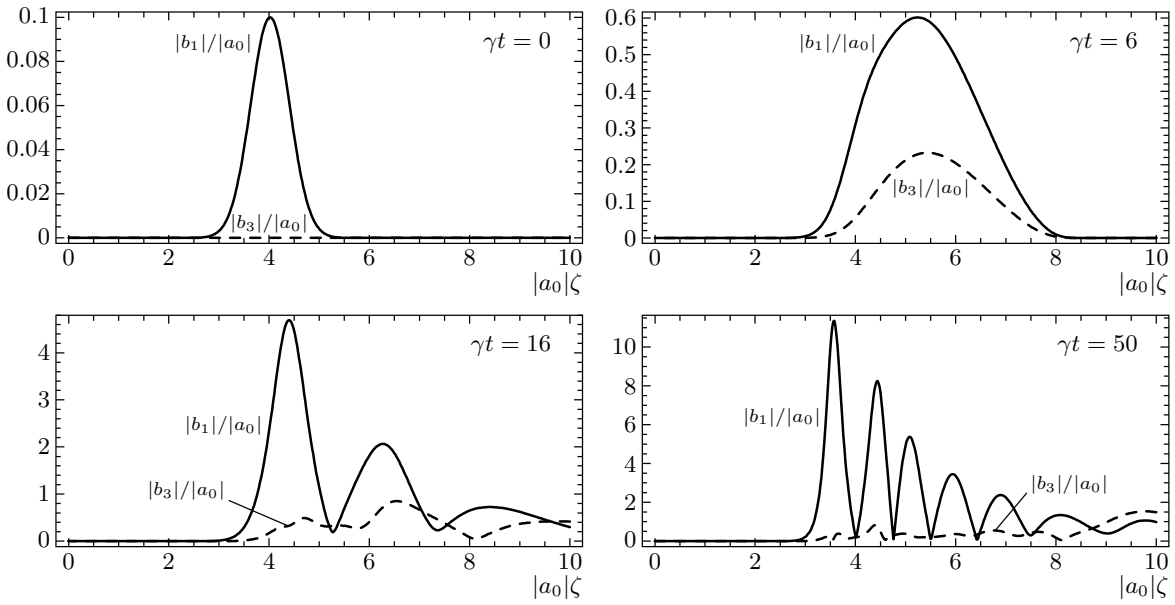

Fig. 3. Evolution of $|b_1(\zeta)|/|a_0|$ (solid line) and $|b_3(\zeta)|/|a_0|$ (dotted line); the planar-waveguide scalar problem; $b_m^{(0)} = 0.1 a_0 \delta_{m1}$, $a_n^{(0)} = a_0 \delta_{n1}$, $R = \pi/\sqrt{a_0}$; $b_2 \equiv 0$ because of symmetry; the shots correspond to $\gamma t \equiv |a_0|\tau = 0, 5, 15, 50$. Strong waveguide dispersion provides nonlinear competition of the modes in the nonlinear regime of amplification. Although the small amplitude b_3 appears at the linear stage, it is left behind the wave envelope b_1 later. Amplification of b_3 is then slowed down by the pump depletion provided by b_1

tends to dominate in the nonlinear stage of amplification, thereby preserving the transverse structure of the pulse.

The evolution of the two lowest modes having the highest amplitudes is shown in Fig. 3. (To show the robustness of the mode competition mechanism, numerical calculations demonstrating the single-mode amplification were performed for $a \sim a_{crit}$.) In this case, the single-mode amplification also continues in the nonlinear regime, ensuring that the problem remains essentially one-dimensional. We can see the formation of the self-similar profile, which represents the attractor of the single-mode operation, similarly to the $1D$ problem. The energy distribution inside the amplified pulse (which determines the effective pulse length) averaged over the capillary cross-section is given in Fig. 4.

The qualitative arguments given above lead to the conclusion that the formation of the single-mode operation regime in the case of a strong waveguide dispersion is stable with respect to fluctuations of the seed pulse. Neither the fluctuations of the pump transverse structure can influence the single-mode operation because all the modes of the pump wave provide approximately equal efficiencies of the energy transfer into the amplified pulse, as discussed in Sec. 4.

The nonlinear competition of the modes constituting the amplified pulse remains efficient only until the higher modes enter the nonlinear stage of amplification. After that, their envelopes catch up with the wave envelope of the first mode and ruin the tail of the single-mode structure (Fig. 5). But the front of the amplified pulse always remains in the linear regime (see also Sec. 3), which provides its single-mode structure.

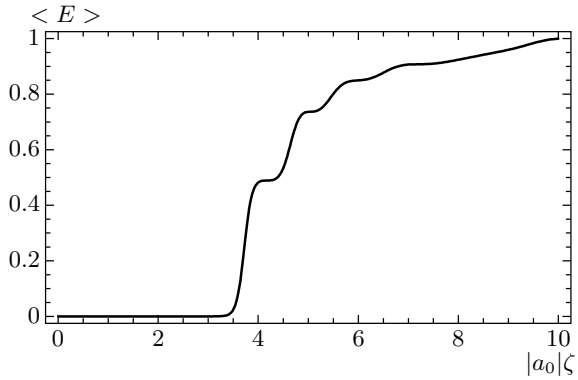

Fig. 4. The normalized energy integral distribution within a quasi-single-mode amplified pulse (averaged over the capillary cross-section): up to 50 % of the pulse total energy is contained within the first peak; the parameters are the same as in Fig. 3, $\gamma t = 40$

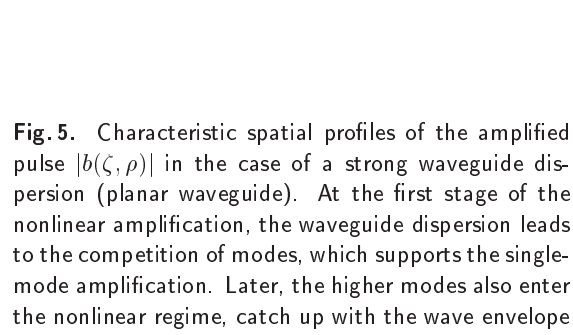

Fig. 5. Characteristic spatial profiles of the amplified pulse $|b(\zeta,\rho)|$ in the case of a strong waveguide dispersion (planar waveguide). At the first stage of the nonlinear amplification, the waveguide dispersion leads to the competition of modes, which supports the single-mode amplification. Later, the higher modes also enter the nonlinear regime, catch up with the wave envelope of the first mode, and ruin the structure of its tail. The front of the pulse always remains single-mode, however, because it always stays in the linear regime, where the growth of the higher modes is suppressed by a strong waveguide dispersion

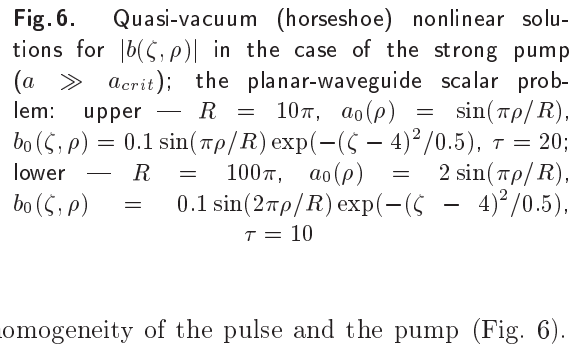

Fig. 6. Quasi-vacuum (horseshoe) nonlinear solutions for $|b(\zeta,\rho)|$ in the case of the strong pump ($a \gg a_{crit}$); the planar-waveguide scalar problem: upper — $R = 10\pi$, $a_0(\rho) = \sin(\pi\rho/R)$, $b_0(\zeta,\rho) = 0.1\sin(\pi\rho/R)\exp(-(\zeta-4)^2/0.5)$, $\tau = 20$; lower — $R = 100\pi$, $a_0(\rho) = 2\sin(\pi\rho/R)$, $b_0(\zeta,\rho) = 0.1\sin(2\pi\rho/R)\exp(-(\zeta-4)^2/0.5)$, $\tau = 10$

In the other limiting case, where the interaction between the pump and the amplified pulse is strong ($\gamma \gg \delta\Omega^{(b)}$, or $a \gg a_{crit}$), the pulse is significantly amplified on a small distance compared to z_R, i.e., before the diffraction effects come into play. The waveguide walls cannot then influence the formation of the pulse structure at the first stage of amplification, and a solution close to those formed in boundless vacuum is produced. Vacuum solutions [6] are shaped as nested horseshoe structures resulting from the transverse inhomogeneity of the pulse and the pump (Fig. 6). On every geometric ray, a self-similar profile is formed with its own $\epsilon_0(\rho)$ (or $\epsilon_{eff}(\rho)$), which determines the longitudinal spatial structure of the pulse at given ρ. At the edges of the amplified pulse, the amplitudes of both **a** and **b** are smaller than in the center of the system, and the longitudinal spatial scales are larger correspondingly.

In the frame moving together with the front of the amplified pulse (at the speed of light), the longitudinal locations of the pulse maxima $\zeta_{max}(\rho)$ are bounded by the position of the front of the seed pulse ζ_0. On the other hand, the nonlinear compression provided by the preferential amplification of the front of the pulse «pushes» the tail of the pulse from behind to $\zeta = \zeta_0$, which implies that ζ_0 represents the limit of $\zeta_{max}(\rho)$ for all ρ. The front of the horseshoe structure therefore

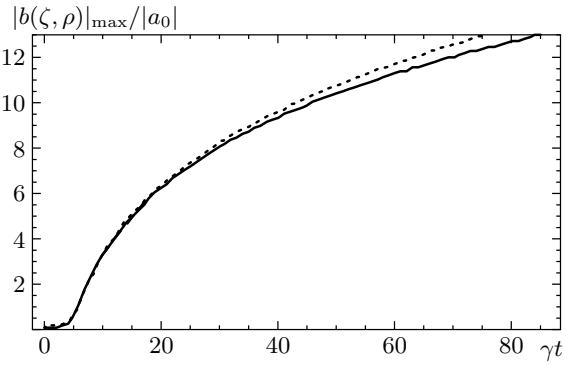

Fig. 8. The maximum amplitude of a horseshoe-type pulse normalized one the amplitude of the pump wave ($|b(\zeta,\rho)|_{max}/|a_0|$) as a function of time $\gamma t \equiv |a_0|\tau$ (solid line). The dotted line represents a $1D$ solution with $\epsilon_{eff}(\tau)$ for $b_0(\zeta, R/2)$ (the same initial conditions as in Fig. 7). The front peak of the amplified pulse grows similarly to the one of the $1D$ self-similar profile with decreasing ϵ_{eff}

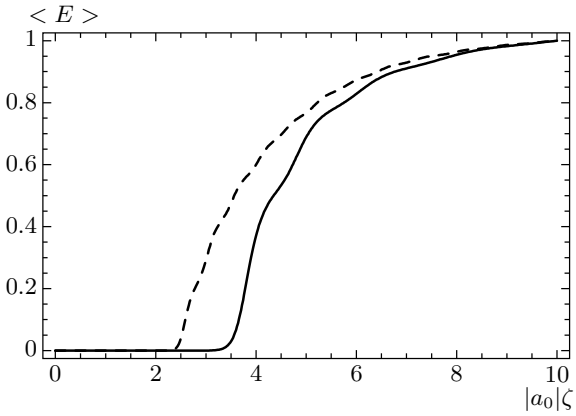

Fig. 9. The normalized energy integral distribution within a horseshoe-type amplified pulse (averaged over the capillary cross-section): $\gamma t \equiv |a_0|\tau = 20$ (solid line) and $\gamma t = 90$ (dashed line); the same parameters as in Fig. 7. For larger γt, the averaged energy distribution becomes a smooth function (cf. Fig. 4), and it is therefore difficult to distinguish the individual peaks of the amplified pulse. On average, the energy is distributed over a length that is significantly larger than the length of the first peak

Fig. 7. Deterioration of the horseshoe solution $|b(\zeta,\rho)|$ as $\tau \to \infty$ and flattening of the front of the amplified pulse (the planar-waveguide scalar problem, $R = 10\pi/\sqrt{a_0}$, $a_0(\rho) = a_0 \sin(\pi\rho/R)$, $b_0(\zeta,\rho) = 0.1a_0 \sin(\pi\rho/R)\exp(-(\zeta-4)^2/0.5)$): $\gamma t \equiv a_0\tau = 20$, 90 correspondingly; dark regions correspond to larger $|b|$

tends to flatten as $\tau \to \infty$.

Although stable on small distances compared to z_R and robust with respect to the structure of the seed (see also Ref. [6]), the horseshoe solution deteriorates inside the waveguide at $z \gtrsim z_R$, where the diffraction becomes significant (Fig. 7). The very front of the horseshoe, however, always remains in the linear regime, and therefore maintains its regular shape. In the center of the waveguide, the front peak of the amplified pulse grows similarly to the self-similar solution of $1D$ problem (16) (Fig. 8), which allows using the $1D$ model for estimating the maximum amplitude of the amplified pulse. The energy distribution inside the amplified pulse (which determines the effective pulse length) averaged over the capillary cross-section is given in Fig. 9. At large t, the averaged energy longitudinal distribution becomes a smooth function (cf. Fig. 4), and it is therefore difficult to distinguish the individual peaks of the amplified pulse. On average, the energy becomes distributed over a length that is significantly larger than the length of the first peak.

6. SUPPRESSING NOISE AMPLIFICATION IN DETUNED INTERACTION

Because of the extreme efficiency of the Raman backscattering, which makes the fast compression possible, delivering the pump wave energy to the seed pulse through the amplifying plasma layer represents a signif-

icant challenge. As the pump traverses the plasma layer towards the seed pulse, the fast Raman backscattering of the pump by thermal Langmuir waves or electromagnetic fluctuations existing inside the plasma layer or coming from outside can lead to a premature pump depletion. The problem is aggravated by the fact that the linear Raman backscattering instability of the pump (responsible for the unwanted noise amplification) has a larger growth rate than its nonlinear counterpart (responsible for the useful amplification of the seed laser pulse).

To see how significantly the thermal fluctuations can limit the maximum amplification gain of the seed pulse, we consider the amplification at the identically zero detuning of the three-wave interaction. After a certain period of time t_m, the amplification gain

$$D_m \sim e^{G_m}, \quad G_m = \gamma t_m,$$

becomes sufficient for thermal fluctuations to deplete the pump wave substantially, and further amplification of the seed pulse is then suppressed. The dimensionless quantity G_m depends on the plasma temperature and does not depend on the amplitude of the pump wave. The maximum amplification of the desired signal with respect to a_0 is then given by

$$\frac{b_{max}}{a_0} \approx \frac{2\,G_m\sqrt{2}}{1+\ln\left(\dfrac{4}{\epsilon_0}\sqrt{2\pi}\right)} \tag{33}$$

and is independent of the amplitude of the pump. For $G_m \approx 20$, the electromagnetic wavelength $\lambda = 1\mu$m, the initial pulse duration 50 fs, and the initial pulse power density $P = 10^{13}$ W/cm^2, we obtain that the maximum amplification that can be achieved in a pump of an arbitrary intensity before the noise is amplified to the level of suppressing the pump is $b_{max}/a_0 \approx 6$.

Nevertheless, through a nonlinear filtering mechanism identified in Ref. [5], it is possible to suppress the unwanted instability of the pump wave without suppressing the desirable seed pulse amplification. The filtering effect occurs because the pumped pulse duration decreases inversely proportional to the pulse amplitude in the nonlinear regime. The pulse frequency bandwidth increases with the pulse amplitude, and the growing nonlinear instability can therefore tolerate larger and larger external detuning from the backscattering resonance. Because the linear instability, i.e., the exponential growth of thermal fluctuations, has a narrower bandwidth, filtering the desired signal can be achieved by arranging for an appropriate combination of the detuning and nonlinear effects. A slight frequency detuning can be equivalently provided either by the pump chirping or by inhomogeneity of the plasma density along the trace of the pulse amplification resulting in variations of the plasma frequency involved in the three-wave resonance condition.

While the exact solution for a delta-pulse amplification problem obtained in Ref. [5] precisely deals with the linear profile of frequency detuning, we use an approximate analysis in this section to describe how the pulse amplification develops in the case of an arbitrary detuning profile. For this, we first consider the linear stage of amplification of a weak pulse b governed by the equation

$$(\partial_\tau - i\delta\omega)(\partial_\tau - \partial_z)b = |a_0|^2 b \tag{34}$$

(without the loss of generality, we temporarily neglect the transverse structure and the polarization of the amplified pulse for qualitative conclusions). Using the quasistatic approximation and assuming the detuning to change slowly along the trace of the pulse propagation, we can treat $\delta\omega$ as a slow function of time τ [5]. We perform the Fourier transformation of Eq. (34),

$$b = \int b_{\Delta k} \exp(i\Delta k z) d\Delta k,$$

and take

$$b_{\Delta k}(\tau) = \psi(\tau) \exp\left(i \int\limits_0^\tau \frac{\delta\omega(\tau') + \Delta k}{2} d\tau'\right), \tag{35}$$

to transform the equation for the amplitude of the pulse spatial harmonic ψ to the form

$$\begin{aligned} &\left[\frac{d^2}{d\tau^2} + w^2(\tau)\right]\psi = 0, \\ &w^2 = i\Omega_\tau + \Omega^2 - |a_0|^2, \quad \Omega = (\delta\omega - \Delta k)/2. \end{aligned} \tag{36}$$

In accordance with the assumption of a smooth detuning profile, we take

$$q(\tau) = \frac{\delta\omega_\tau}{|a_0|^2} \ll 1.$$

Outside the regions where Ω^2 is close to $|a_0|^2$, the effective «frequency» w can be estimated as

$$w = \sqrt{\Omega^2 - |a_0|^2} + \frac{i\Omega_\tau}{2\sqrt{\Omega^2 - |a_0|^2}}, \tag{37}$$

and the amplification gain is given by

$$D \sim e^G, \quad G \approx \int \operatorname{Im} w \, d\tau$$

in the WKB approximation. At $\Omega^2 > |a_0|^2$, G depends on the length of the trace of the pulse propagation logarithmically, and the amplification gain is therefore negligible in the adopted approximation. Thus, the total amplification gain is given by

$$G \approx \int\limits_{\Omega^2<|a_0|^2} \sqrt{|a_0|^2 - \Omega^2(\tau)}\, d\tau. \qquad (38)$$

For the detuning monotonically changing along the trace of the pulse propagation, Eq. (38) can be written as

$$G \approx \frac{2}{|a_0|} \int\limits_{\Omega^2<|a_0|^2} \sqrt{1 - \frac{\Omega^2}{|a_0|^2}}\, \frac{d\Omega}{|q(\Omega)|} \le \frac{\pi}{|q_{min}|}, \qquad (39)$$

where $|q_{min}|$ stands for the minimum rate of the detuning evolution on the trace of amplification. As can be seen from Eq. (39), the upper limit of the total amplification gain on the entire trace of the pulse propagation is independent of Δk (included in the definition of Ω over which the integration is performed). For $q = \text{const}$, we have

$$D \sim \exp(\pi/|q|),$$

as obtained in Ref. [5], and therefore, D itself is independent of Δk.

We can also generalize Eqs. (38), (39) to the case of oblique propagation of the pulses, describing the amplification of the electromagnetic noise coming from outside the system. The only difference is then that the group velocity of the amplified harmonic differs from the speed of light, which results only in a redefinition of Δk and does not affect the form of the final result in Eqs. (38) and (39) if $q(\tau)$ is calculated relative to the actual trajectory of the amplified pulse.

Equations (38) and (39) predict that each harmonic of a given frequency and a wavenumber is amplified only inside the region where the three-wave resonance conditions are satisfied in the sense that $\Omega^2 < |a_0|^2$ (or, in dimensional variables, $(\delta\omega - c\Delta k)^2/4 < \gamma^2$). The idea of the approach given here is similar to the one proposed by Rosenbluth and Pilia (see, e.g., Ref. [12]), who estimated the total linear amplification gain for stationary waves in an inhomogeneous medium with the wavenumber detuning but with the temporal resonance condition satisfied exactly. The difference between the two cases is that instead of the wavenumber detuning, the frequency detuning is important for the Raman pulse amplification in inhomogeneous plasmas. For the Raman backscattering in a cold plasma, the wavenumber resonance condition is satisfied automatically, because a plasma wave is allowed to have an arbitrary wavenumber, although it oscillates at a certain frequency ω_p.

The conclusion that follows from the obtained result is that the detuning profile along the pulse amplification trace can be chosen such that the noise amplification is suppressed above a certain level determined by Eq. (38). Monotonically changing the detuning allows a stronger suppression, because there exists only one region for a given harmonic where the amplification occurs. In this case, the requirement for the characteristic $|q|$ to ensure that the noise is not amplified up to the transition to the nonlinear stage but the desired signal is ($\int b(z)dz \gtrsim 1$, see Refs. [1, 3]) can be formulated as

$$\frac{\pi}{G_m} \ll |q| \ll \frac{\pi}{\ln \dfrac{1}{\epsilon_0}}, \qquad (40)$$

$$q = \frac{c}{\gamma^2}\frac{\partial\,\delta\omega}{\partial z} \approx \frac{10^{14}}{L_\delta \lambda P},$$

$$\frac{1}{L_\delta} = \frac{1}{\omega_p}\frac{\partial\omega_p}{\partial z} + \frac{1}{2\omega_p c}\frac{\partial\omega_a}{\partial t}, \qquad (41)$$

where the characteristic spatial scale L_δ of the detuning evolution due to the plasma inhomogeneity (the first term in Eq. (41)) and the pump chirping (the second term) is measured in cm, the wavelength λ is measured in microns, and the pump power is measured in $\mathrm{W/cm^2}$.

The next problem is how the frequency detuning influences the desired signal amplification in the nonlinear regime. We now show that it does not as long as these variations remain sufficiently smooth. To prove this, we consider the change of variables

$$\begin{aligned} a &= \tilde{a}, \\ b &= \tilde{b}\exp(i\delta\omega(\tau + z)), \\ f &= \tilde{f}\exp(-i\delta\omega(\tau + z)), \end{aligned} \qquad (42)$$

leading to the following $1D$ form of Eqs. (6)–(8):

$$\begin{aligned} &\partial_\tau\tilde{a} + \partial_z\tilde{a} = \tilde{b}\tilde{f}, \\ &\partial_\tau\tilde{b} - \partial_z\tilde{b} - i(\tau + z)qa_0^2\tilde{b} = -\tilde{a}\tilde{f}^*, \\ &\partial_\tau\tilde{f} = -\tilde{a}\tilde{b}^*. \end{aligned} \qquad (43)$$

These equations are equivalent to Eqs. (6)–(8) with zero detuning if $q = 0$. The physical meaning of the formal change of variables (42) is as follows. The carrier frequencies of the seed pulse and the plasma wave are chosen such that the three-wave resonance condition is satisfied locally,

$$\tilde{\omega}_a - \tilde{\omega}_b(z) = \tilde{\omega}_f(z), \qquad (44)$$

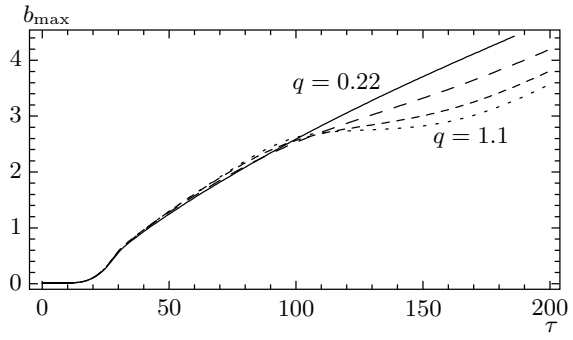

Fig. 10. Pulse-detuned nonlinear amplification $b_{max}(\tau)$ at different frequency detuning profiles $\delta\omega(\tau) = 2(1+\mathrm{th}((\tau-100)/\tau_0))$: $q = 2/(a_0^2\tau_0) = 0.22,\ 0.44,\ 0.74,\ 1.1$; $a_0 = 0.3$. (The larger q is, the lower the graph goes at $\tau > 100$.) For $q \sim 1$, the amplification efficiency decreases in the region where the detuning evolves relatively fast ($100 < \tau < 150$), while at small q (e.g., for $q = 0.22$), the amplification proceeds exactly as in the case of zero detuning for all τ

where

$$\tilde{\omega}_b(z) = \omega_b + \delta\omega(z), \quad \tilde{\omega}_f(z) \equiv \omega_p(z)$$

are functions of space, and the carrier frequency of the pump wave $\tilde{\omega}_a = \omega_a$ is left unchanged. It is only the gradient of the detuning that enters Eqs. (43), and the constant part of $\delta\omega$ enters the initial conditions for the seed pulse only.

In the frame moving together with the seed pulse ($\zeta = z + \tau$), in the quasistatic approximation [3], the basic equations can be written as

$$\begin{aligned} &2\partial_\zeta \tilde{a} = \tilde{b}\tilde{f}, \\ &\partial_\tau \tilde{b} - i\zeta q a_0^2 \tilde{b} = -\tilde{a}\tilde{f}^*, \\ &\partial_\zeta \tilde{f} = -\tilde{a}\tilde{b}^*, \end{aligned} \tag{45}$$

which implies that the term corresponding to the detuning is negligible compared to the nonlinear drive when the overfall of the detuning $\Delta(\delta\omega)$ on the length of the pulse is small compared to $1/\tau$. Because

$$\Delta(\delta\omega) \sim q a_0^2 \zeta_{pulse},$$

where the characteristic length of the pulse is $\zeta_{pulse} \sim \sim 1/a_0^2\tau$ at the nonlinear stage of interaction [3], the condition of negligible detuning becomes

$$|q| \ll 1. \tag{46}$$

The obtained condition for efficient amplification of short pulses was tested numerically. It can be seen from Fig. 10 that for $q \sim 1$, the amplification efficiency decreases in the region where the detuning evolves relatively fast, while at small q (e.g., for $q = 0.22$), the amplification proceeds exactly as in the case of zero detuning for all τ, exactly as predicted by the qualitative arguments given above.

The obtained results imply that for short pulses, amplification can be efficient on the entire trace of the interaction with the pump wave. The integral variation of $\delta\omega$ (or the maximum frequency detuning amplitude experienced by the pulse on its trace of amplification) does not significantly influence the amplification efficiency if the detuning evolves smoothly along the trace of amplification. Condition (46) only requires the bandwidth of the wave envelope $\Delta\omega_b$ to grow due to the nonlinear compression sufficiently fast for the local-resonance frequency $\omega_a - \omega_p(z)$ to lie within the amplification line. For growing $|q|$ that approaches unity, the interaction becomes nonresonant, and the pulse amplification ceases. If q decreases, the pulse amplification develops similarly to the solution with a constant detuning. The degenerate case where $q =$ const and the amplification efficiency depends on the amplitude of the initial pulse logarithmically is discussed in detail in Refs. [1, 5].

In a real experiment, transverse plasma inhomogeneities must be taken into account in addition to the detuning provided by pump chirping and longitudinal variations of the plasma density. It is important that the dependence of $\delta\omega$ on the transverse location lowers the sensitivity of the interaction efficiency to the average detuning (over the cross-section). In the $1D$ problem, as shown above, the pulse amplification can be entirely suppressed by large gradients of the plasma density. But in the case where the plasma density also changes in the transverse direction, a radial position ρ_* such that $\delta\omega(\rho_*) = 0$ exists at every cross-section of the pulse trajectory. The pulse can extract energy from the pump wave in the vicinity of $\rho = \rho_*$, although the interaction remains inefficient far from this point. This local pulse amplification cannot be entirely suppressed by large detuning that might exist at other radial positions. This fact determines a higher robustness of the pulse amplification in inhomogeneous plasmas in $2D$ or $3D$ systems than in the $1D$ case. In the case where the amplification occurs inside a capillary, the pulse energy is mixed in the transverse direction because of the reflection of electromagnetic waves from the walls of the waveguide, which eventually results in a nonlocal amplification of the waveguide eigenmodes, i.e., in the amplification of the entire pulse.

Sample parameters for the Raman amplification inside an oversize dielectric capillary

Wavelength λ	1 μm
Electron density n_e	10^{19} cm^{-3}
ω/ω_p	10
Radius of capillary R	50λ
Diffraction length z_R	0.16 cm
Inverse decay rates α_{nm}^{-1}	60/40 cm
Trace of amplification	1.2 cm
Pulse duration	40 ps
a_0	0.006
Pump intensity	10^{14} W/cm^2
Pump power	$4 \cdot 10^9$ W
Amplification length c/γ	0.12 mm
Seed pulse duration	100 fs
Seed pulse intensity	10^{14} W/cm^2
ϵ_0	0.25
Amplification factor b_{max}/a_0	20
Amplified pulse intensity	$3.5 \cdot 10^{16}$ W/cm^2
Amplified pulse power	$1.4 \cdot 10^{12}$ W

The refraction index of capillary walls is taken $n = 1.5$; the pump wave intensity corresponding to $a = a_{crit}$ is $1.4 \cdot 10^{11}$ W/cm^2, and the amplified pulse is therefore of the horseshoe type; the inverse spatial decay rates α_{nm}^{-1} are calculated for the two most slowly decaying modes.

7. DISCUSSION

Characteristic parameters of the proposed Raman-backscattering pulse amplification experiment are given in the Table. For the wavelength $\lambda \approx 1\mu$m and the radius of the capillary sufficiently large for the radiation energy losses to be negligible, the single-mode operation can only be provided by low pump intensities, which do not allow significant amplification on a reasonable (centimeter size) interaction length. At pump intensities higher than the critical one, multi-mode solutions are formed.

The parameters given in the Table correspond to the maximum possible amplification gain at the given wavelength and the electron density limited by such effect as the Langmuir wave breaking and the forward Raman scattering instability [1, 3], which remained out of the scope of our study and represent the field of further research in the context of the $3D$ Raman scattering problem. As regards the modulation instability, it is expected to be suppressed for the proposed parameters because the critical power of the amplified pulse self-focusing $P_{crit} = 17(\omega/\omega_p)^2$ GW [3] is equal to $1.7 \cdot 10^{12}$ W, which is less than the power of the amplified pulse.

In summary, using a dielectric capillary for channeling laser radiation in a Raman amplifier provides a significant advantage as regards maintaining high interaction efficiency at distances larger than the diffraction length, which allows obtaining higher intensities of the output radiation. In addition, various mechanisms of selective mode discrimination and nonlinear competition of capillary modes are provided by the transverse waveguide dispersion, but cannot be achieved in boundless vacuum. Although the presence of the capillary walls can influence the structure of the pulse, it does not alter the amplification of the front peak of the pulse, which carries a significant amount of the total energy of the pulse.

We find that depending on the intensity of the pump, two possible regimes of operation can be realized within a capillary, namely, the single-mode and the multi-mode pulse amplification. For a low pump wave intensity, when the single-mode operation is possible, the problem admits the resonant mode approach that we develop in this paper. We also develop the linear theory of pulse amplification inside a capillary by generalizing the $1D$ linear problem. Contrary to the intuitive expectations, we show that the pulse amplification efficiency is not critically sensitive to the transverse structure of the pump wave, and therefore, both lower and higher modes of the pump provide approximately the same amplification rates of the seed pulse.

We generalize the mechanism of avoiding the pump wave instability (resulting in the noise amplification) by chirping the pump wave or inhomogeneous plasma profile along the trace of the pulse propagation [5] in the case of an arbitrary smooth detuning profile. We show that as the noise amplification can be suppressed by detuning, the latter does not alter the amplification of the desired pulse as long as the detuning profile remains sufficiently smooth. We conclude that guiding laser pulses through the capillary provides an additional robustness of the interaction efficiency with respect to transverse inhomogeneities of the plasma density.

The authors thank A. A. Balakin for help in performing numerical simulations and A. N. Stepanov and V. A. Mironov for fruitful discussions. The work was supported by the Russian Foundation for Basic Research (grants 01-02-17388, 02-02-06258).

APPENDIX

Waveguide modes of a dielectric capillary

The waves channelled by a dielectric capillary can be separated into the surface and the waveguide-type waves [13]. A slow surface wave propagates without dissipation inside the dielectric walls of the tube with the wavenumber

$$h = \sqrt{\epsilon k^2 + \kappa_\epsilon^2},$$

where ϵ is the dielectric permittivity, $\kappa_\epsilon \sim 1/d$ is the wave transverse wavenumber, and d is the width of the capillary wall. Outside the dielectric, the field of the surface wave decays exponentially with the spatial decrement

$$\kappa_0 = \sqrt{h^2 - k^2} = \sqrt{(\epsilon - 1)k^2 - \kappa_\epsilon^2} \sim k$$

for $kd \gg 1$. Therefore, at the distance of several wavelengths from the wall, the surface wave field essentially equals zero, and as regards the interaction of pulses inside the capillary, the impact of the surface wave field can be neglected.

Waveguide-type waves propagate inside the capillary, with the channeling provided by reflection of waves from the inner surface of the capillary dielectric wall. For paraxial propagation ($k \gg 1/R$), the reflection coefficients of most of the waveguide-type waves are close to unity. The only exception is given by several waves with transverse wavenumbers close to the resonant ones, for which the dielectric walls of the given width are transparent. Unless the capillary transverse sizes are maintained with high precision, which is not usually the case for the applications similar to the Raman amplifier, these resonances disappear because of the random corrugation of the wall surface. In this case, all the waveguide-type waves can therefore be treated as slowly decaying ones.

In the first-order approximation, the boundary conditions for the electric and magnetic fields on the inner wall of the dielectric capillary (under the assumption of the negligible decay rate) are given by

$$E_r(R) = H_r(R) = 0$$

(see [13]). The transverse structure of the electric field is then given by

$$\boldsymbol{\psi}_{m,\,n,\pm1} = \frac{\mathbf{p}_{\pm1}}{\sqrt{\pi}} \frac{J_{m\pm1}(\mu_{m\pm1,\,n} r/R)}{R J_m(\mu_{m\pm1,\,n})} \exp(im\theta), \quad (47)$$

where

$$\mathbf{p}_{\pm1} = \frac{\boldsymbol{\theta}^{(0)} \pm i\mathbf{r}^{(0)}}{\sqrt{2}} = \frac{(\mathbf{y}^{(0)} \pm i\mathbf{x}^{(0)}) \exp(\pm i\theta)}{\sqrt{2}}$$

are unit polarization vectors and $\mu_{m\pm1,\,n}$ are the roots of the Bessel functions ($J_{m\pm1}(\mu_{m\pm1,\,n}) = 0$). Eigenmodes (47) are normalized such that

$$\langle \boldsymbol{\psi}_{m_1,\,n_1,\,j_1} | \boldsymbol{\psi}_{m_2,\,n_2,\,j_2} \rangle = \delta_{m_1,\,m_2} \delta_{n_1,\,n_2} \delta_{j_1,\,j_2}, \quad (48)$$

where $m_{1,2}$ stand for the azimuthal indices, $n_{1,2}$ stand for the radial indices, and $j_{1,2}$ determine the polarization of the modes. The decay rate α_n for the n-th mode can be obtained in the second order of the perturbation theory under the assumption of the known transverse structure of the mode. Explicit expressions for α_n are given in Ref. [9] (see also Sec. 4).

REFERENCES

1. V. M. Malkin, G. Shvets, and N. J. Fisch, Phys. Plasmas **7**, 2232 (2000).
2. G. A. Mourou, C. P. J. Barty, and M.D. Perry, Phys. Today, **51**, 22 (1998).
3. V. M. Malkin, G. Shvets, and N. J. Fisch, Phys. Pev. Lett. **82**, 4448 (1999).
4. G. Shvets, N. J. Fisch, A. Puknov, and J. Meyer-ter-Vehn, Phys. Pev. Lett. **81**, 4879 (1998).
5. V. M. Malkin, G. Shvets, and N. J. Fisch, Phys. Rev. Lett. **84**, 1208 (2000).
6. G. M. Fraiman, N. A. Yampolsky, V. M. Malkin, and N. J. Fisch, submitted to Phys. Plasmas (2002).
7. N. S. Vorobev, A. B. Grudinin, E. M. Dianov, A. M. Prokhorov, D. V. Khaidarov, I. Y. Khruschev, and M. Y. Shchelev, Pis'ma v Zh. Eksp. Teor. Fiz. **44**, 17 (1986).
8. A. B. Grudinin, E. M. Dianov, D. V. Korobkin, A. M. Prokhorov, V. N. Serkin, and D. V. Khaidarov, Pis'ma v Zh. Eksp. Teor. Fiz. **45**, 260 (1987).
9. E. A. J. Marcatili and R. A. Schmeltzer, Long Dist. Opt. Comm. **43**, 1783 (1964).
10. A. G. Litvak, Zh. Eksp. Teor. Fiz. **30**, 344 (1970).
11. W. L. Kruer, *The Physics of Laser Plasma Interactions*, Addison-Wesley Publ. (1988).
12. A. A. Galeev and R. Z. Sagdeev, *Voprosy Teorii Plazmy*, **7**, 3 (1973).
13. L. A. Wainstein, *Electromagnetic waves*, Radio i Svyaz, Moscow (1988).